Available online at www.sciencedirect.com
ScienceDirect
Journal of Power Sources 164 (2007) 196–202
JOURNAL OF POWER SOURCES
www.elsevier.com/locate/jpowsour

Demonstration of a residence time distribution method for proton exchange membrane fuel cell evaluation

J. St-Pierre [a,*,1], A. Wong [a], J. Diep [b], D. Kiel [b]

[a] *Ballard Power Systems, 9000 Glenlyon Parkway, Burnaby, BC, Canada V5J 5J9*
[b] *Coanda Research and Development Corporation, 110A-3430 Brighton Avenue, Burnaby, BC, Canada V5A 3H4*

Received 22 June 2006; received in revised form 25 August 2006; accepted 15 September 2006
Available online 13 November 2006

Abstract

The volume sensitive residence time distribution method is ideally suited for the study of liquid water and ice formation within operating proton exchange membrane fuel cells. Sensitivity was demonstrated with the use of simulated water drops within the flow field channel (machined obstructions) yielding a linear correlation in the 0–20% volume obstruction range between measured and theoretical hydraulic volumes. The correlation was independent of obstruction spatial distribution but dependent on gas flow rate. Sensitivity was also demonstrated by varying the amount of liquid water within a gas diffusion electrode resulting in a linear correlation in the 7–44% void volume obstruction range between normalized time difference between the points at which the tracer concentration has decayed by 20 and 90% of the steady-state value prior to the tracer injection interruption and measured gas diffusion electrode liquid water content. Sensitivity to liquid water obstructions was maintained using an operating fuel cell and two different gas diffusion media with relatively similar transport properties but further work is needed to separate flow field from gas diffusion electrode contributions. The usefulness of the residence time distribution is also demonstrated for other applications, including gas crossover through the proton exchange membrane, flow distribution uniformity and gas diffusion electrode compressibility/deformation.

Keywords: Proton exchange membrane fuel cells; Residence time distribution; Water management; Flow field obstruction; Gas diffusion electrode liquid water content

1. Introduction

A recent review has highlighted the need to develop new measurement methods to characterize the presence of liquid and solid water within proton exchange membrane fuel cells (PEMFCs) considering their potential negative effects on performance, including freezing periods, and degradation [1]. The United States Department of Energy has recognized the validity of such an endeavor by currently providing significant research funds [2]. Residence time distribution (RTD) techniques, which are volume sensitive [3], are ideally suited for PEMFC study, since liquid and solid water modify the space available to distribute reactants through both flow field channels and gas diffusion electrodes (GDEs).

Few RTD studies were devoted to fuel cells [4–6]. Among these, none were developed for an operating PEMFC. This situation prompted recent research efforts resulting in a CO_2 tracer/infrared detector based system [7]. RTD system components and procedure (tracer injection, tracer detection, calibration, pressure correction, data scaling) and performance characteristics (response time, accuracy, sensitivity, repeatability) were discussed in detail and constituted the main focus with little emphasis given to potential applications.

Previously developed PEMFC RTD systems [7] were used and results covering a range of applications are presented. Focus is given to the detection of volume changes within flow field channels and gas diffusion electrodes. Other potential applications are highlighted, including gas crossover through the membrane, flow distribution and compressive pressure (to effect a seal between the bipolar plate and membrane/electrode assemblies, MEAs).

* Corresponding author.
E-mail address: jeanst@engr.sc.edu (J. St-Pierre).
[1] Present address: Future Fuels^{TM} Initiative, Department of Chemical Engineering, University of South Carolina, Swearingen Engineering Center, 301 Main Street, Columbia, SC 29208, USA.

0378-7753/$ – see front matter © 2006 Elsevier B.V. All rights reserved.
doi:10.1016/j.jpowsour.2006.09.103

Nomenclature

c	tracer concentration (mol m^{-3})
$\bar{c}$	average tracer concentration (mol m^{-3})
E_t	normalized tracer concentration
Q	volumetric flow rate (m^3 s^{-1})
t	time (s)
t_h	hydraulic time (s)
t_x	time required for the tracer concentration to reach $100 - x\%$ of the tracer step amplitude (s)
$\bar{t}$	average RTD normalized time (centroid based)
V	hydraulic volume (m^3)
x	percentage (%)

Greek symbol

θ	normalized time

2. Experimental

Two proprietary Ballard Power Systems fuel cell designs were used (Mk5, Mk9) either in a non-operational or an operational mode. The Mk9 design was also modified for some experiments to minimize the volume associated with the distance separating the tracer injection/detection points and the fuel cell active area (connection tubing, valves, fuel cell reactant manifold), with the objective to increase sensitivity to phenomena occurring within the fuel cell. The modification was implemented by adding a bipolar plate next to the standard oxidant bipolar plate allowing in-plane rather than through-plane (via the manifolds) reactant supply and withdrawal. Fig. 1a illustrates one end of the modified plate, showing connection tubes for reactant supply/withdrawal, tracer injection/sampling and pressure measurement. Tube connection fittings and a seal material plug to reduce manifold volume of the oxidant bipolar plate are also shown in Fig. 1b. For some other experiments, the oxidant flow field design was modified by reducing the cumulative flow field channel volume with the objective to simulate the presence of liquid water droplets. Several hypothetical water droplet distributions and total volume changes were simulated to determine RTD method sensitivity. This approach was selected because it offered an independent estimate for the volume change that was correlated with RTD characteristics. Fig. 2 summarizes the different flow field designs. Finally, for the tests simulating the presence of liquid water within the gas diffusion electrode, the cell design was modified to ensure minimal error during water content measurements. For this purpose, water transfer between fuel cell compartments was eliminated using a GDE adjacent to a flat and impermeable carbon plate. Additionally, water loss was minimized weighing the entire oxidant flow field plate/GDE/blank carbon plate assembly rather than only the GDE. Several proprietary MEA designs were used.

The most advanced RTD system consisted of a CO_2 injection syringe activated by a computer controlled stepper motor traverse. This arrangement led to repeatable and continuous, step or pulse tracer injections. A two-channel model LI-7000 CO_2/H_2O analyzer manufactured by LI-COR was used for tracer detection. Signal saturation by liquid water was avoided using several methods (adding dry gas for dilution, favoring mixing within tube connection fittings). The two identical sampling lines located at the fuel cell inlet and outlet were simultaneously operated, which allowed for simple tracer concentration and time calibration with the presence of rotameters within the dilution loops and pressure transducers at the inlet of the capillary tracer sampling tubes (flow rates adjustment to the same values for both dilution and sampling streams). More details related to the development and operation of the RTD system are provided elsewhere (RTD system D [7]). Results obtained using other RTD systems [7] are also presented and are identified using the same notation (RTD system A–D).

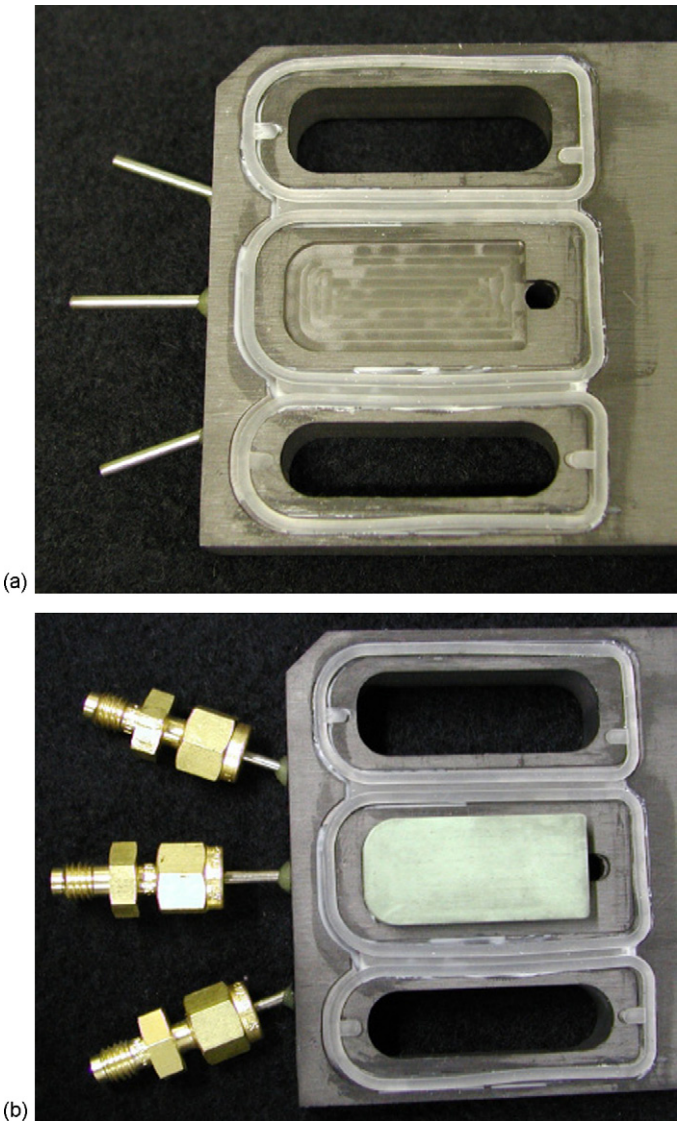

Fig. 1. Insert Mk9 bipolar plate designed to reduce dead volume between tracer sampling locations and active fuel cell area. (a) Plate modification with reduced oxidant manifold volume and, tubes for reactant supply/withdrawal, tracer injection/sampling and pressure measurement and (b) plate modification with tube connection fittings and seal material oxidant manifold plug.

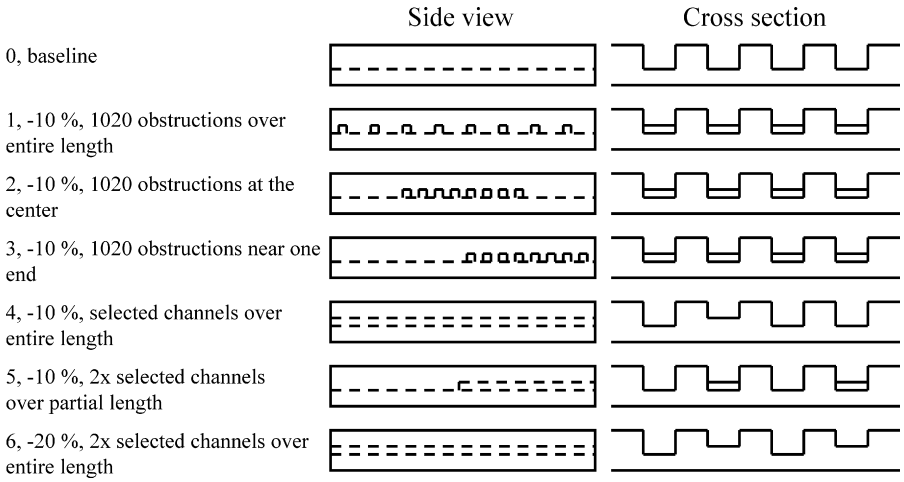

Fig. 2. Modified Mk9 oxidant flow field bipolar plate designs with reduced flow volumes simulating liquid water drop distributions. Drawings are not to scale. Obstruction size is 0.22 mm × 3.24 mm × 0.79 mm, 34 channels per plate.

3. Results and discussion

3.1. Water management application

Recent progress achieved with flow visualization methods [8–11] has revealed that flow field channels are either partly filled with liquid water droplets or entirely clogged (thus blocking reactant transport) depending on operating conditions. Although water drop size distributions were not studied in detail, estimated values can be obtained from the flow field channel dimensions. Flow field channel cross-sections varied from 1 to 1.5 mm^2. This range is consistent with the partial obstruction size of 0.56 mm^3 that was used for the modified oxidant bipolar plates (Fig. 2). The case of selected and fully blocked flow field channels was not investigated since it is not desirable during fuel cell operation. In term of location, water drops were observed either along the entire length of the flow field or segregated within the outlet section (equivalent to one third of the flow field channel length). These observations are also consistent with the obstruction schemes that were studied (Fig. 2) including the additional case of water drops located within the central part of the flow field length.

A non-operational cell and a tracer pulse injection were used to obtain RTDs for the different oxidant bipolar plates to, respectively, focus on the simulated water drop obstruction effect and maximize sensitivity to flow field phenomena [7]. Fig. 3 illustrates resulting inlet and outlet RTDs. The timing difference between the pulses essentially represents the volume separating the sampling points as the gas travels through the cell. The change in pulse shape is attributable to various dispersion phenomena, which is outside the scope of the present paper. In Fig. 3, the time was scaled using the hydraulic time derived from the known volume between sampling points and gas flow rate:

$$\theta = \frac{t}{t_h} = \frac{tQ}{V} \tag{1}$$

This scaling explains the location of the outlet RTD, centered at a value of ~1. The concentration was also scaled using the area under the respective RTDs:

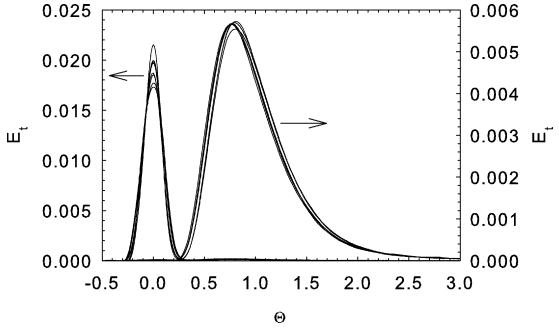

Fig. 3. Fuel cell inlet and outlet RTDs obtained with a baseline Mk9 oxidant bipolar plate, added bipolar plate to reduce hydraulic volume and RTD system D. Non-operating cell, 10 l air min^{-1} at standard conditions.

$$E_t = \frac{c}{\int_0^\infty c\,dt} \tag{2}$$

The timing difference between inlet and outlet RTDs was calculated using centroid based time estimates:

$$\bar{t} = \frac{\int_0^\infty ct\,dt}{\int_0^\infty c\,dt} \tag{3}$$

The timing difference derived from Eq. (3) was assumed to be equal to the hydraulic time, leading to a measured value for the hydraulic volume using the experimental gas flow rate. The measured hydraulic volumes were scaled using the baseline flow field design hydraulic volume and compared to the target volume changes (Fig. 4). A correlation was found between the measured and target flow field volume changes despite the purposeful use of only 10–20% volume reductions indicating a potential for high sensitivity. Furthermore, it appears that location and distribution of the blockages do not have a significant effect (an unexpected benefit). Presumably, the gas can circulate around the blockages through the gas diffusion electrode. Therefore, the entire volume occupied by the gas phase is accessible to the flow. By comparison, the gas flow rate appears to have a significant effect (the lower gas flow rate curve is located above the

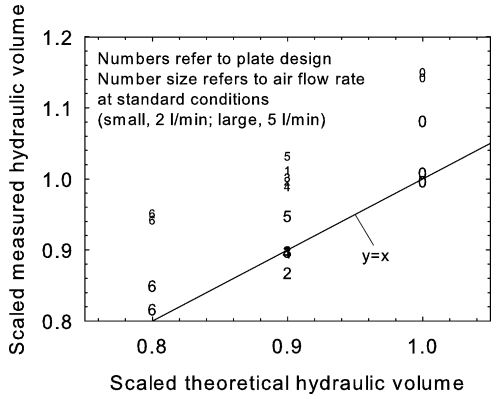

Fig. 4. Comparison between scaled measured hydraulic volumes and theoretical hydraulic volumes.

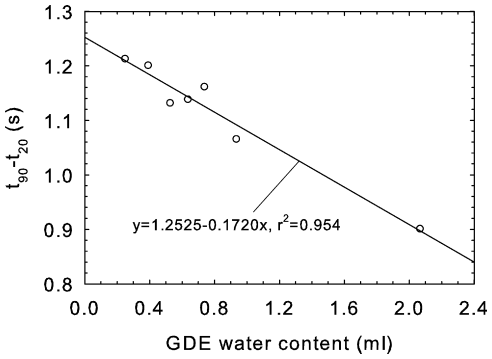

Fig. 6. Comparison between the normalized time difference between the points at which the tracer concentration has decayed by 90 and 20% of the steady-state value prior to the tracer injection interruption and GDE liquid water content.

ideal curve). This may be the result of a change in flow regime, which could be confirmed with a more detailed study (smaller incremental changes in gas flow rates).

The potential of the RTD method to detect liquid water within the GDE was also investigated by first soaking a sample in an alcohol/water solution. The GDE was subsequently allowed to dry until the alcohol had evaporated and inserted in the non-operational cell equipped with a baseline oxidant flow field plate and a blank plate. The fuel cell was not operated and a negative step pulse injection (saturation of the cell with tracer before its supply is shut off) were used to, respectively, focus on the liquid water obstructions effect within the porous material and maximize sensitivity to GDE phenomena [7]. Dry gas was first circulated for some time to reduce the liquid water within the GDE by evaporation. Thereafter, an RTD measurement was completed, the gas supply was shut off, the fuel cell was dismantled and the entire oxidant flow field plate/GDE/blank plate assembly was weighed to provide an independent measurement of the liquid water content. The RTD and weighing procedures were repeated until the GDE liquid water content range of interest was covered. In Fig. 5, the time was scaled using Eq. (1) whereas the concentration was scaled using the steady-state value prior to the tracer injection interruption:

$$E_t = \frac{c}{\bar{c}_{t<0}} \tag{4}$$

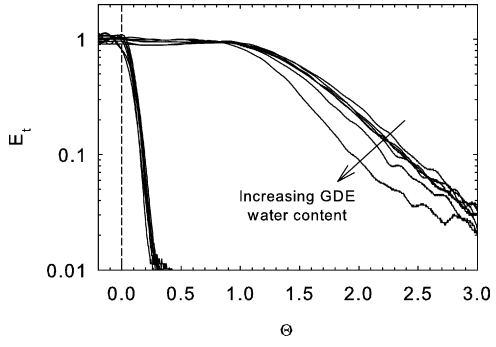

Fig. 5. Fuel cell inlet and outlet RTDs obtained with a baseline Mk9 oxidant bipolar plate, added bipolar plate to reduce hydraulic volume, a GDE and blank bipolar plate instead of an MEA, and RTD system D. Non-operating cell, 5 l air min^{-1} at standard conditions.

In this case, the outlet concentration decays at a normalized time of ∼1. It is observed that inlet RTDs overlap whereas outlet RTDs are displaced to larger normalized time values as the GDE is dried. This is consistent with a larger hydraulic volume and consequently larger hydraulic time. Fig. 5 data were further analyzed by measuring the normalized time difference between the points at which the tracer concentration has decayed by 20 and 90% of the steady-state value prior to the tracer injection interruption (t_{20} and t_{90}). Fig. 6 illustrates $t_{90} - t_{20}$ values as a function of the amount of liquid water within the GDE. A significant correlation was found even if data below t_{40}, which are located within a range outside the CO_2 detector dynamic range causing signal distortions [7], were used. The measurement method sensitivity is better appreciated by computing the GDE approximate void volume, which is equal to 4.5 cm^3 (294 cm^2 × 0.022 cm × 0.7). Since the GDE water content was varied between 0.3 and 2 cm^3, the investigated range corresponds to 7–44% of the GDE void volume.

Since correlations were found between RTD characteristics, flow field blockages and liquid water in the GDE, additional tests were completed with an operational fuel cell. For this case, two different gas diffusion media with similar transport properties (MEA A had an in-plane permeability equal to ∼76% of the MEA B value) were used in an attempt to determine the sensitivity of the RTD method. The step method was selected again to emphasize the GDE related phenomena. Fig. 7a and b shows the resulting inlet and outlet RTDs for 30 and 150 A currents. For each case, differences between MEAs are observed and are presumably due to GDE liquid water content. Additionally, a current effect is observed since differences between MEAs are larger at 30 than 150 A. Normalized time differences for the outlet RTDs ($t_{95} - t_{10}$) were computed and plotted as a function of flow field channel Reynolds number (Fig. 8). The flow field channel hydraulic diameter was selected as the Reynolds number characteristic length. Both MEAs are affected by the current magnitude and suggest the presence of two opposing forces ruling GDE water content, water production and liquid water removal [12–14]. For low currents, the production of liquid water is small and consequently, the GDE is relatively dry as indicated by the larger $t_{95} - t_{10}$ value. However, as the current and water production are increased, the

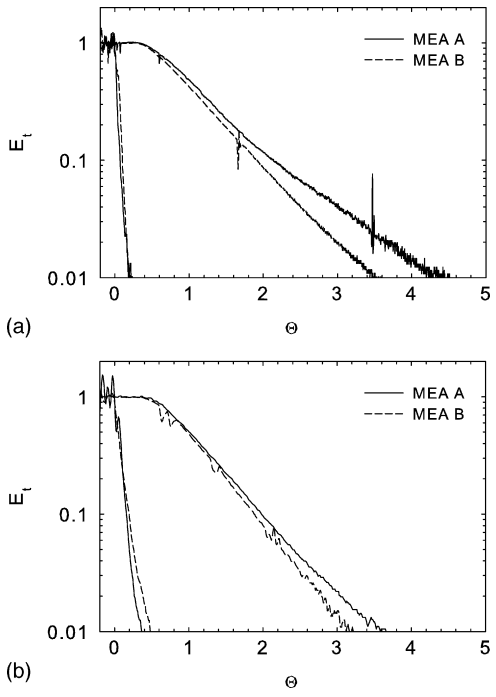

Fig. 7. Fuel cell inlet and outlet RTDs obtained with a baseline Mk9 oxidant bipolar plate and RTD system D. Operating cell: (a) 30 A and (b) 150 A.

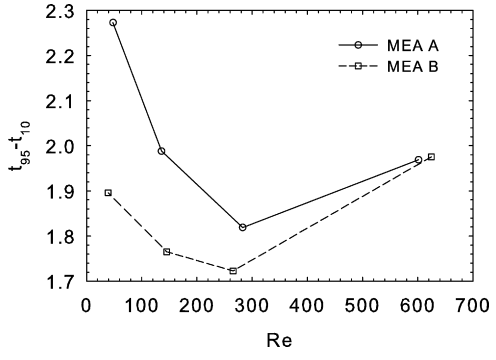

Fig. 8. Comparison between the normalized time difference between the points at which the tracer concentration has decayed by 90 and 5% of the steady-state value prior to the tracer injection interruption and flow field channel Reynolds number.

GDE becomes increasingly wetter (there is a drop in $t_{95} - t_{10}$) since the flooded pores are still largely disconnected (liquid water cannot escape as a result of capillary forces). At even larger currents, water production is significant but is largely compensated by the action of capillary forces for removal (flooded pores are largely connected) resulting in an effectively drier GDE (there is an increase in $t_{95} - t_{10}$). The present operating fuel cell RTD characterization results indicate that the method is sensitive to GDE design. Further tests are required to confirm these results since other effects are at play and may affect RTD interpretation including reactant consumption and product generation which would affect both local gas flow rates and residence time. Additionally, interpretation methods need to be developed to separate the flow field channel effects from the GDE effects.

3.2. Other applications

Emphasis was given to measurement of liquid water within operating fuel cells using an RTD method. Three other fuel cell applications of the RTD method, further increasing its value, are presented, which do not necessarily rely exclusively on volume sensitivity.

Gas diffusion through proton exchange membranes is dependent on water content, temperature and nature of the gas [15]. In principle, this behavior should also apply to a tracer such as CO_2 although solubility and transport properties in proton exchange membranes could not be found (emphasis is usually given to the oxygen and hydrogen reactants). An experiment was conducted by injecting a pulse tracer on the non-operating fuel cell cathode side inlet but with tracer detection located at the anode side outlet. Fig. 9 illustrates the results, which demonstrate that CO_2 does diffuse through the MEA and that the RTD system sensitivity is sufficient for its detection. The validity of the measurements is indicated by a centroid based normalized hydraulic time greater than 1, revealing the retarding effect of gas diffusion in a solid state. The differential pressure effect also contributes to support the validity of the measurements with increasing tracer crossover with an increase in cathode compartment pressure and corresponding solubility in the polymer. Similar experiments could be performed with an operating cell and minimal invasiveness (a significant advantage). As an example, the effect of current density could be investigated and the crossover results correlated to the membrane water content (drier membranes would lead to a greater retarding effect on tracer detection). These experiments could confirm similar results obtained with impedance spectroscopy [16].

Reactant flow distribution within flow field bipolar plates is an important consideration in terms of power density and active area utilization optimization which ultimately also influences cost [17,18]. Evaluation methods include current distribution tools to evaluate performance uniformity [19–21]. RTD methods have only recently been used to achieve the same objective for liquid feed direct methanol fuel cell anodes [5] but more development is required for gaseous reactants. Especially since current distribution tools are relatively complex and expensive, and fuel cell design dependent (a significant disadvantage [1]).

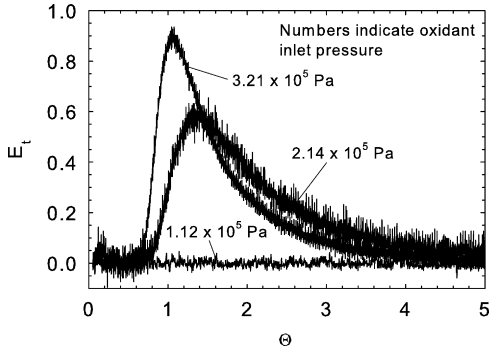

Fig. 9. Fuel cell anode outlet RTDs obtained with a Mk5 design and RTD system A as a result of tracer injection in the cathode compartment. Non-operating cell, air/N_2, 2.1/2.4 l min^{-1} at standard conditions, variable/1.28 × 10^5 Pa.

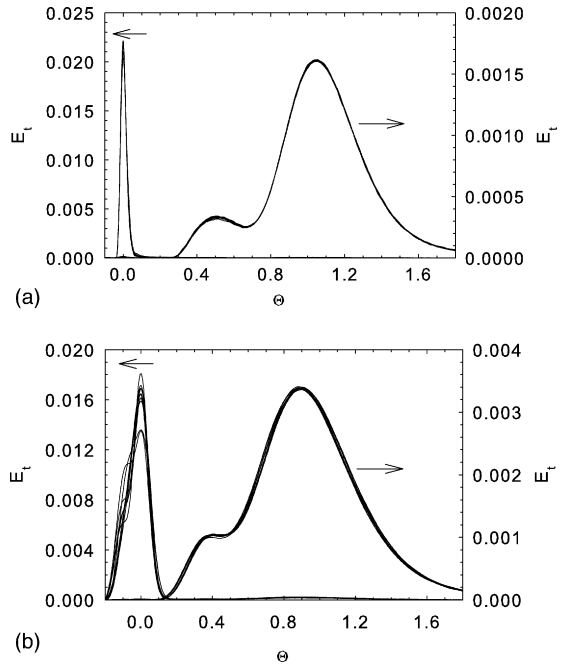

Fig. 10. Fuel cell inlet and outlet RTDs obtained with a modified Mk9 oxidant bipolar plate (design 2, Fig. 2), added bipolar plate to reduce hydraulic volume and RTD system D. Non-operating cell: a, 21 N_2 min^{-1} at standard conditions and b, 51 N_2 min^{-1} at standard conditions.

During flow field obstruction tests (Fig. 2), an unexpected outlet RTD feature appeared in some cases (Fig. 10) indicating the presence of bypass flow with the appearance of a secondary peak earlier than the main peak. This observation highlights the qualitative but rapid diagnostic capabilities of the RTD method [3]. In this particular case, the bypass flow is not easy to explain since all the channels were partially blocked to the same level (symmetric design). This interesting result suggests the importance of using the RTD method to assess flow field design behavior even for simple designs and the need for more experiments to postulate an explanation. Fig. 10 also shows the effect of an increasing gas flow rate on the bypass flow, which decreases in magnitude (the secondary peak merges with the main peak). Flow field designs should therefore be tested over the complete operating range.

Fuel cells are typically composed of a series of alternating bipolar plates and MEAs compressed together to seal each of the reactant and coolant compartments. The compression pressure is an important parameter, which requires optimization to minimize contact resistance while avoiding structural failure of the GDE porous structure [22]. The compression pressure is especially important for continuous manufacturing of MEAs based on flexible GDEs to reduce cost. Flexible GDE deformation and movement within the flow field channel is a potential issue negatively affecting pressure drop and fuel cell system efficiency. Pressure drop and unit cell cross-sections can be used to assess the level of GDE penetration within the flow field channels. Pressure drop measurements are simple but cannot discriminate between flow field channel and GDE free volume changes. Microscopic cross-section analysis is destructive and time consuming. An experiment was conducted with an MEA based on a flexible GDE to assess the sensitivity of the RTD method. A tracer step was used to focus on the GDE. Fig. 11 illustrates the effect of compression pressure using a bladder mechanism. The results show that an increase in pressure leads to a translation of the RTD to smaller normalized time values. This is consistent with a reduction of the hydraulic volume either as the result of GDE intrusion into the flow field channels and/or collapse of the porous material (loss of void volume). Partial validation is provided by Fig. 12, which shows an increase in flow field pressure drop with compression indicative of the presence of partial obstructions. Additional experiments are required to determine the level of discrimination that can be achieved between flow field intrusion and porous material void volume reduction. Similar tests could also be performed using a differential pressure between anode and cathode compartments.

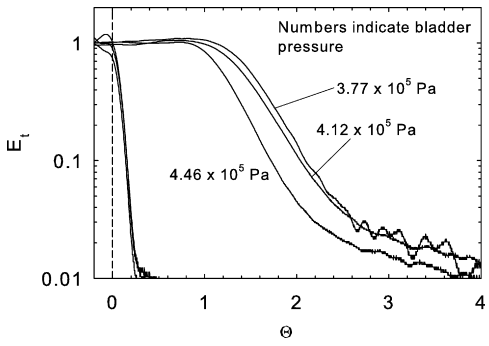

Fig. 11. Fuel cell inlet and outlet RTDs obtained with a baseline Mk9 oxidant bipolar plate, added bipolar plate to reduce hydraulic volume, MEA based on a flexible GDE and RTD system D. 3.08 × 10^5 Pa cathode and anode pressure.

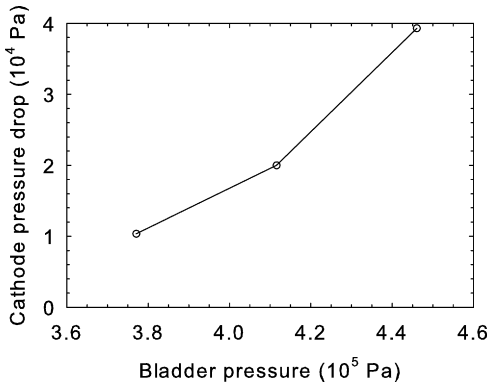

Fig. 12. Cathode flow field pressure drop as a function of bladder pressure obtained with a baseline Mk9 oxidant bipolar plate, added bipolar plate to reduce hydraulic volume and MEA based on a flexible GDE. 3.08 × 10^5 Pa cathode and anode pressure.

4. Conclusion

Several operating fuel cell applications were identified for the previously developed RTD method. Significant work remains with respect to method development and validation, and fuel cell characterization. In particular, significant attention should be given to data interpretation to relate RTD characteristics to fuel cell design parameters of interest. The development of mathematical models represents a potential approach to address this

problem. All these activities are necessary to ensure maximum benefits from detailed characterization studies including mapping the operating condition and unit cell design effects on flow field channel and GDE liquid water content.

References

[1] J. St-Pierre, in: S. Paddison, K. Promislow (Eds.), Device and Materials Modeling of Polymer Electrolyte Membrane Fuel Cells, Springer, submitted for publication.
[2] www.eere.energy.gov/hydrogenandfuelcells/about.html.
[3] H.S. Fogler, Elements of Chemical Reaction Engineering, second ed., Prentice Hall, 1992.
[4] M. Duduković, H. Weinstein, D.Y.C. Ng, J. Appl. Electrochem. 1 (1971) 219.
[5] U. Krewer, Y. Song, K. Sundmacher, V. John, R. Lübke, G. Matthies, L. Tobiska, Chem. Eng. Sci. 59 (2004) 119.
[6] M. Boillot, S. Didierjean, F. Lapicque, Chem. Eng. Sci. 60 (2005) 1187.
[7] J. Diep, D. Kiel, J. St-Pierre, A. Wong, Chem. Eng. Sci., in press.
[8] K. Sugiura, M. Nakata, T. Yodo, Y. Nishiguchi, M. Yamauchi, Y. Itoh, J. Power Sources 145 (2003) 526.
[9] K. Tüber, D. Pócza, C. Hebling, J. Power Sources 124 (2003) 403.
[10] A. Hakenjos, H. Muenter, U. Wittstadt, C. Hebling, J. Power Sources 131 (2004) 213.
[11] X.G. Yang, F.Y. Zhang, A.L. Lubawy, C.Y. Wang, Electrochem. Solid-State Lett. 7 (2004) A408.
[12] J.H. Nam, M. Kaviany, Int. J. Heat Mass Transfer 46 (2003) 4595.
[13] U. Pasaogullari, C.-Y. Wang, J. Electrochem. Soc. 151 (2004) A399.
[14] U. Pasaogullari, C.-Y. Wang, Electrochim. Acta 49 (2004) 4359.
[15] K. Broka, P. Ekdunge, J. Appl. Electrochem. 27 (1997) 117.
[16] T. Abe, H. Shima, K. Watanabe, Y. Ito, J. Electrochem. Soc. 151 (2004) A101.
[17] A.C. West, T.F. Fuller, J. Appl. Electrochem. 26 (1996) 557.
[18] S.W. Cha, R. O'Hayre, Y. Saito, F.B. Prinz, J. Power Sources 134 (2004) 57.
[19] X.-G. Yang, N. Burke, C.-Y. Wang, K. Tajiri, K. Shinohara, J. Electrochem. Soc. 152 (2005) A759.
[20] Z. Liu, Z. Mao, B. Wu, L. Wang, V.M. Schmidt, J. Power Sources 141 (2005) 205.
[21] A. Hakenjos, C. Hebling, J. Power Sources 145 (2005) 307.
[22] S.-J. Lee, C.-D. Hsu, C.-H. Huang, J. Power Sources 145 (2005) 353.